Observable effects of poles and shadow poles in coupled-channel systems

B. C. Pearce* and B. F. Gibson
Theoretical Division, Los Alamos National Laboratory, Los Alamos, New Mexico 87545
(Received 19 September 1988)

Using separable potentials in a coupled-channel Lippmann-Schwinger equation, we investigate the motion of poles on the different Riemann sheets and their observable effects as the coupling strength is varied. Only in the weak-coupling limit can one determine in which uncoupled channel the pole originated by the sheet on which it lies. Cusp structure versus resonance peak as one crosses a threshold is found to depend on the distance of the pole from the physical sheet. Resonance poles in each uncoupled channel can produce double-loop Argand plots similar to those seen in πN P_{11} amplitude analysis.

I. INTRODUCTION

An important question in coupled-channel scattering problems is what effect poles on the many Riemann sheets will have on the scattering observables. Within any given calculational framework it is often relatively straightforward to locate all poles in a specified energy region. However, understanding of a given system is aided as much by intuition as by calculation. To develop intuition in this case requires an understanding of how poles on the various sheets affect the scattering observables. It has been recognized for some time (although perhaps often overlooked) that in a multichannel system, a resonance pole near the physical region can be accompanied by shadow poles on sheets far removed from the physical region. Eden and Taylor[1] demonstrated the existence of these poles by considering the zero-coupling limit of a two-channel system. If a pole exists on one of the two sheets describing a single-channel system then it will appear on two of the four sheets that describe the two-channel system with zero coupling. For weak coupling, determination of the specific sheets on which a pole appears identifies with which channel the resonance is associated.

Recently, Hale *et al.*[2] extracted the pole positions from their R-matrix fit to the coupled $n\alpha$-dt system and found such a pole–shadow-pole pair associated with the $J^\pi=\frac{3}{2}^+$ resonance in ^{5}He. From the sheet on which the shadow pole resided, they used the Eden and Taylor analysis to infer that the cross section structure is basically due to an n-α resonance instead of the usual interpretation in terms of a d-t resonance. However, the examples we present show that this inference is not necessarily valid once one departs from the weak-coupling regime. We exhibit several examples where the shadow-pole trajectory actually crosses from one sheet to another as the coupling is increased. Since the shadow pole that Hale *et al.* find is much closer to the real axis than is the resonance pole, it is quite possible that it has just changed sheets. Hence, it is impossible to determine on which sheet the shadow pole originated without following the pole trajectories back to the zero-coupling limit.

In order to add to the intuitive level of understanding of the role of poles and shadow poles in coupled-channel systems, we have considered a model in which the interactions are described by separable potentials with Yamaguchi-type form factors. The t matrix for this system can be calculated on any specified Riemann sheet by careful evaluation of the various integrals. Poles are then found by searching for zeros in the determinant of the τ function for some complex energy.

We should point out that the use of coupled-channel models to examine the interplay of nearby poles and thresholds on scattering observables is not new. For example, Lovas and Dénes[3] used an exactly soluble Faddeev treatment to conclude that threshold anomalies can occur when there is strong overlap between a resonance pole and a threshold. Kloet and Tjon[4] used a similar formalism to examine in some detail the nature of two dibaryon candidates, concluding that proper treatment of the $N\Delta$ threshold is essential in such an analysis. The present work continues in this vein with particular emphasis on the (hitherto somewhat ignored) shadow pole.

Cusp effects at the opening of a new channel manifest themselves most strongly in the s wave. Frazer and Hendry[5] give an example that illustrates a transition from cusp to (rounded) resonance peak as the pole crosses from a sheet that cannot be easily reached from the physical region to a sheet that can. We verify this finding and also give an example (from a parametrization of the Λ-Σ system[6]) where the transition from cusp to peak results from a gradual lengthening of the path from the pole to the physical region. Conventional wisdom suggests that cusps occur near the opening of a threshold of a channel that has an antibound state. This example demonstrates that a cusp can develop at the opening of a channel containing a bound state, when the coupling is sufficiently strong.

When we consider p waves, we can consider the interesting case where we initially have a narrow pole above the second channel threshold. Our first observation here is that the shadow pole is free to cross the threshold cuts along the real axis above the second channel threshold, changing sheets as it does so. We also observe an interesting relation between the sheet on which the shadow pole lies and the structure of the phase shifts.

 ©1989 The American Physical Society

Interesting phase shifts result when two channels that both possess resonance poles are coupled. When the original poles are positioned such that the second channel pole lies a bit higher in energy than the first channel pole, and the coupling is weak, then it is possible to obtain a small loop in the Argand diagram superimposed on a larger, typical resonance loop. The structure produced looks remarkably similar in form to the Karlsruhe-Helsinki P_{11} πN amplitudes.[7]

The final example we investigate is that of an s wave coupled to a d wave, as one has in the $n\alpha$-dt system. Looking at this case serves to confirm that effects we saw in the $l=1$ partial wave are general and do not depend on the particular choice of partial wave.

The remainder of the paper is organized as follows. In Sec. II we describe the separable potential coupled-channel model we are using, paying particular attention to describing how the t matrix is calculated on an arbitrary sheet of energy. Section III contains a detailed description of each of the cases we considered, which have already been briefly outlined. Finally, we present our conclusions in Sec. IV.

II. THE SEPARABLE, MULTICHANNEL t MATRIX

Our purpose here is to define clearly the model we are using and to illustrate how the t matrix is calculated on any arbitrary Riemann sheet of energy. The t matrix is obtained by solving the coupled-channel Lippmann-Schwinger equation, which after partial-wave projection is

$$t_{\alpha\beta}(p,\,p';E)=v_{\alpha\beta}(p,\,p')+\sum_{\gamma}\int_0^{\infty}dp''\,p''^2 v_{\alpha\gamma}(p,p'')\frac{1}{E-\Theta_\gamma-p''^2/2\mu_\gamma}t_{\gamma\beta}(p'',p';E)\ . \tag{2.1}$$

Here Θ_γ is the threshold energy of channel γ and μ_γ is the reduced mass. The relation between the S matrix and the t matrix is

$$S_{\alpha\beta}=\delta_{\alpha\beta}+2iT_{\alpha\beta}\ , \tag{2.2}$$

where

$$T_{\alpha\beta}=-\pi\sqrt{\mu_\alpha k_\alpha \mu_\beta k_\beta}\,t_{\alpha\beta}(k_\alpha,\,k_\beta;E)\times\theta(E-\Theta_\alpha)\theta(E-\Theta_\beta)\ , \tag{2.3}$$

and k_α is the on-shell momentum in channel α

$$k_\alpha=\sqrt{2\mu_\alpha(E-\Theta_\alpha)}\ . \tag{2.4}$$

The range of $\arg k_\alpha$ for complex energies is discussed later. The θ functions ensure that contributions to the S matrix only come from open channels. The N-channel potential we use is an $N\times N$ matrix with elements

$$v_{\alpha\beta}(p,p')=f_\alpha(p)\lambda_{\alpha\beta}f_\beta(p')\ . \tag{2.5}$$

The form factors are taken to be simple Yamaguchis

$$f_\alpha(p)=\frac{p^{l_\alpha}}{(1+p^2/\beta_\alpha^2)^{l_\alpha+1}}\ , \tag{2.6}$$

where l_α is the angular momentum of channel α. The t matrix is then

$$t_{\alpha\beta}(p,p';E)=f_\alpha(p)\tau_{\alpha\beta}(E)f_\beta(p')\ , \tag{2.7}$$

where

$$[\tau^{-1}(E)]_{\alpha\beta}=(\lambda^{-1})_{\alpha\beta}-\delta_{\alpha\beta}I_\alpha(E)\ . \tag{2.8}$$

The positions of poles are determined by the condition

$$\det(\tau^{-1}(E))=0\ . \tag{2.9}$$

The integral $I_\alpha(E)$ is the key to the multisheeted nature of t and is given by

$$I_\alpha(E)=\int_0^{\infty}dp\frac{p^2 f_\alpha^2(p)}{E-\Theta_\alpha-p^2/2\mu_\alpha}\ . \tag{2.10}$$

The end-point singularity in the integrand at $E=\Theta_\alpha$ gives rise to a square-root branch point in $I_\alpha(E)$. Hence we talk about being on either the top or bottom sheet of the α threshold. On the top sheet $0\le\arg k_\alpha<\pi$ while on the bottom sheet $\pi\le\arg k_\alpha<2\pi$. For the case of $l_\alpha=0$ and $l_\alpha=1$, $I_\alpha(E)$ can be easily calculated analytically using the residues of all of the poles of the integrand. However, the integrand poles at $p=\pm i\beta_\alpha$ are of order $2l_\alpha+2$ and the task of obtaining an analytic expression for their residue for $l_\alpha\ge 2$ is somewhat daunting. Hence for $l_\alpha\ge 2$ we compute the integral numerically. For $l_\alpha<2$ we have

$$I_{(l_\alpha=0)}(E)=\frac{\pi\mu_\alpha\beta_\alpha^3}{2(k_\alpha+i\beta_\alpha)^2} \tag{2.11}$$

and

$$I_{(l_\alpha=1)}(E)=\frac{\pi\mu_\alpha\beta_\alpha^5(k_\alpha^2+4i\beta_\alpha k_\alpha-\beta_\alpha^2)}{16(k_\alpha+i\beta_\alpha)^4}\ . \tag{2.12}$$

The difference in $I_\alpha(E)$ on the two sheets arises from the difference in the definition of $\arg k_\alpha$.

When the integral is performed numerically care must be taken to avoid the poles in the integrand at $p=\pm k_\alpha$ and $p=\pm i\beta_\alpha$. By tracing their movements as E encircles the threshold twice, we can choose the contour in such a way that either the top or bottom sheet is selected. (In the following discussion we assume that $\Theta_\alpha=0$.) For physical (i.e., on the top sheet) energies $E=E_R+i\varepsilon$ with $E_R>0$, it is well known that performing the integral along the contour shown in Fig. 1(a) (i.e., a ray in the lower-half momentum plane) gives the correct result. As E is moved from this point in a counterclockwise semicircle, the poles at $\pm k_\alpha$ move as indicated by the dotted curve of Fig. 1(a). At the end point of this path (corre-

sponding to negative, real E on the top sheet) the poles lie on the imaginary axis so that the contour can be continuously deformed to that shown in Fig. 1(b) without crossing any singularities. With the contour in this position we have now exposed the lower-half plane of the top sheet. As we continue to move E smoothly from the end point of the path of Fig. 1(b) onto the path of Fig. 1(c) we move onto the second sheet of energy. To ensure that the pole at $-k_\alpha$ does not get too close to the integration contour we deform the contour back to the lower momentum plane. However, this time we must pick up the clockwise residue of the pole at $p=-k_\alpha$. When the energy again reaches the negative real axis we deform the contour to that shown in Fig. 1(d), retaining the residue of the pole at $-k_\alpha$. At the end point of the path shown in Fig. 1(d) we are back to the same point as the beginning point of the path of Fig. 1(a). To illustrate this, we show in Fig. 1(e) the effect of deforming the contour back to the same position it was in Fig. 1(a). As we see we now also pick up the clockwise residue of the pole at $p=k_\alpha$. However, it is easy to show that [provided $f^2(-p)=f^2(p)$] the two residues cancel. Hence Figs. 1(a) and (e) correspond to the same situation. This demonstrates the square-root nature of the branch point.

In summary then, we have

$$I_\alpha(E_{\text{top}})=\int_C dp\frac{p^2f_\alpha^2(p)}{E-\Theta_\alpha-p^2/2\mu_\alpha} \tag{2.13}$$

and

$$I_\alpha(E_{\text{bottom}})=\int_C dp\frac{p^2f_\alpha^2(p)}{E-\Theta_\alpha-p^2/2\mu_\alpha} -2\pi i\mu_\alpha k_\alpha f_\alpha^2(-k_\alpha)\,, \tag{2.14}$$

where the contour C is as shown in Fig. 1(a) if $\text{Im}(E)\geq 0$ and as in Fig. 1(b) if $\text{Im}(E)<0$. The last term in Eq. (2.14) is the residue at $p=-k_\alpha$.

In the case of N coupled channels, there are N such integrals and, since the energy can be on the top or bottom sheet of each associated threshold independently, there are 2^N sheets. We use an N character string composed of the letters t and b (for top and bottom) as a subscript to E to signify on which sheet of each threshold the energy lies. Thus, for a two-channel case, $E_{[tb]}$ is an energy on the top sheet of the first channel and bottom sheet of the second channel while $E_{[bt]}$ is on the bottom sheet of the first channel and top sheet of the second channel. While acknowledging the undesirability of introducing yet another notation for referring to the various sheets, we have found this notation easy and illuminating to use. The correspondence between this notation, that of Eden and Taylor[1] and the conventional sheet I,II,III,IV notation (see, for example, Ref. 5) is illustrated for the case of two channels in Table I. One of the strengths of this notation is the ease of determining the interconnection of the sheets. The simple rule is that if the branch cut associated with threshold α is crossed then the letter in position α changes. For example, in the two-channel case, above both thresholds sheet $[tt]$ is connected to $[bb]$ while $[tb]$ is connected to $[bt]$. Between the two thresholds $[tt]$ is connected to $[bt]$ and $[bb]$ is connected to $[tb]$.

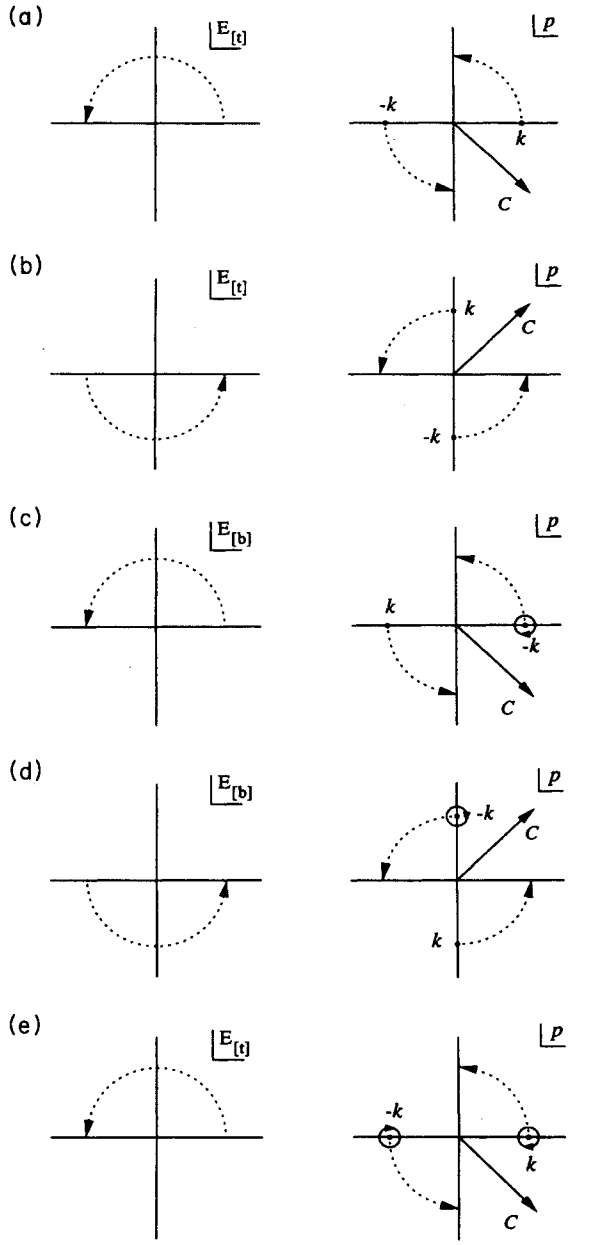

FIG. 1. The movement of the integrand poles at $p=\pm k$ (dotted curves in the momentum plane) corresponding to the indicated movement in the energy plane. Also shown is the integration contour C to be used for each energy region.

Since this paper is concerned with the motion of poles as the coupling strength between channels is varied, it is instructive to examine the ramifications of taking the zero-coupling limit (i.e., $\lambda_{\alpha\beta}=0$ if $\alpha\neq\beta$). In this limit, the condition for a pole [Eq. (2.9)] becomes

$$\prod_\alpha[\lambda_\alpha^{-1}-I_\alpha(E)]=0\,. \tag{2.15}$$

We note that the computation of $I_\alpha(E)$ only requires

TABLE I. Correspondence between various sheet labeling schemes.

This work	Eden and Taylor (Ref. 1)	Frazer and Hendry (Ref. 5)
$[tt]$	P	I
$[bt]$	$U_{(1)}$	II
$[tb]$	$U_{(2)}$	IV
$[bb]$	$U_{(1,2)}$	III

knowledge of which sheet of the α threshold we are on—the value of $I_\alpha(E)$ will be the same no matter what the choice of sheets in channels other than the α channel. Hence, if there is a pole in channel α at energy E_R [i.e., $\lambda_\alpha^{-1}-I_\alpha(E_R)=0$] on some sheet of channel α, then there will be a total of 2^{N-1} poles. For example, in the two-channel case, if there is a pole associated with the bottom sheet of the first channel at energy E_R then there will be poles in the two-channel system at $E_{R[bt]}$ and $E_{R[bb]}$. If the pole were associated with the second channel then we would have poles at $E_{R[tb]}$ and $E_{R[bb]}$. Of course, as the coupling between the channels is turned on, the poles on the various sheets can move apart in energy. Eden and Taylor[1] used the term *shadow poles* to describe these extra poles on unphysical sheets that accompany the usual resonance pole. It is not always clear, however, which should be called the pole and which the shadow pole. For example, if the real part of E_R in the first case mentioned above is close to the second channel threshold, then the pole at $E_{R[bt]}$ is close to the physical region when approached from below the second threshold while $E_{R[bb]}$ is nearby when approached from above the threshold. In this case, the designation of one as the pole and the other as the shadow pole is somewhat arbitrary.

III. SOME CASE STUDIES

The main objective of this paper is to point out some of the somewhat unusual things that can happen to poles in a coupled-channel system and their ramifications for physical observables. In particular, we are interested in what happens as the coupling between channels is varied for cases where there is a pole in only one channel in the limit of zero coupling. We attacked this problem by first finding parameters λ and β that produced a pole at a chosen location in the one-channel case. Two such parameter sets were combined (along with some threshold for the second channel) to produce an uncoupled two-channel t matrix with poles and shadow poles at known positions. As the coupling strength λ_{12} was incrementally increased the pole positions were followed by searching for zeros of $\det\tau^{-1}$ at each parameter value. Below are the results of several such analyses that produced interesting results. The first case reiterates the observations of Frazer and Hendry[5] while, to the best of our knowledge, the remaining examples involving p and d waves have not been previously explored.

A. Two coupled s waves

Frazer and Hendry[5] considered a model with two coupled s waves. We can produce results similar to theirs by considering a case where, in the zero-coupling limit, channel 1 has antibound-state poles that are far from the region of interest (parameter set S_1 from Table II) while channel 2, with a threshold of 3 MeV, has an antibound state that lies between the two thresholds (parameter set S_2). That is, the only relevant poles are a pole and its shadow pole on the real axis between the two thresholds on sheets $[tb]$ and $[bb]$. However, since $[tb]$ and $[bb]$ are connected at that point, we could equally consider there

TABLE II. Single-channel parameters and their poles. The reduced masses to be used in conjunction with these parameter sets are $m_\Lambda m_N/(m_\Lambda+m_N)=509.826$ MeV for sets labeled ΛN, $m_\Sigma m_N/(m_\Sigma+m_N)=524.704$ MeV for sets labeled ΣN, and $m_N/2=469.455$ for all other sets. The ΛN threshold is 2054.5 MeV while for ΣN it is 2128.3 MeV. Parameter sets labeled ΛN and ΣN are taken from Ref. 6 with appropriate modification for our propagator convention. Poles further than 100 MeV from the origin are not listed.

Name	l	λ (fm^{2l+2})	β (fm^{-1})	Poles
S_1	0	−0.043 956 9	1.978 08	$(-30,0)_{[b]}$
S_2	0	−0.134 349	1.630 46	$(-1,0)_{[b]}$
S_3	0	−0.221 596	1.475 18	$(-1,0)_{[t]}$
ΛN_A	0	−0.078 124 4	1.106 87	$(-7.773,0)_{[b]}$
ΣN_A	0	−0.081 446 5	2.701 16	$(-0.464,0)_{[b]}$
ΛN_B	0	0.043 480 5	0.951 80	$(-28.79,\pm28.36)_{[b]}$
ΣN_B	0	−0.300 228	1.278 90	$(-4.307,0)_{[t]}$
ΛN_C	0	0.097 558 7	0.875 22	$(-19.12,\pm34.44)_{[b]}$
ΣN_C	0	−0.918 709	0.533 48	$(-1.960,0)_{[t]}$
P_1	1	−0.018 988 2	1.439 88	$(-30,\pm30)_{[b]}$
P_2	1	$-0.340\,495\times10^{-4}$	39.759 5	$(4.0,\pm0.1)_{[b]}$
P_3	1	$-0.124\,051\times10^{-3}$	25.837 1	$(3.0,\pm0.1)_{[b]}$
P_4	1	−0.034 584 0	3.901 28	$(5.0,\pm1.5)_{[b]}$
P_5	1	−0.386 660	1.744 71	$(1.0,\pm0.3)_{[b]}$
D_1	2	−0.027 730 1	3.319 24	$(4.0,\pm0.1)_{[b]}$ $(-21.57,\ 0)_{[b]}$

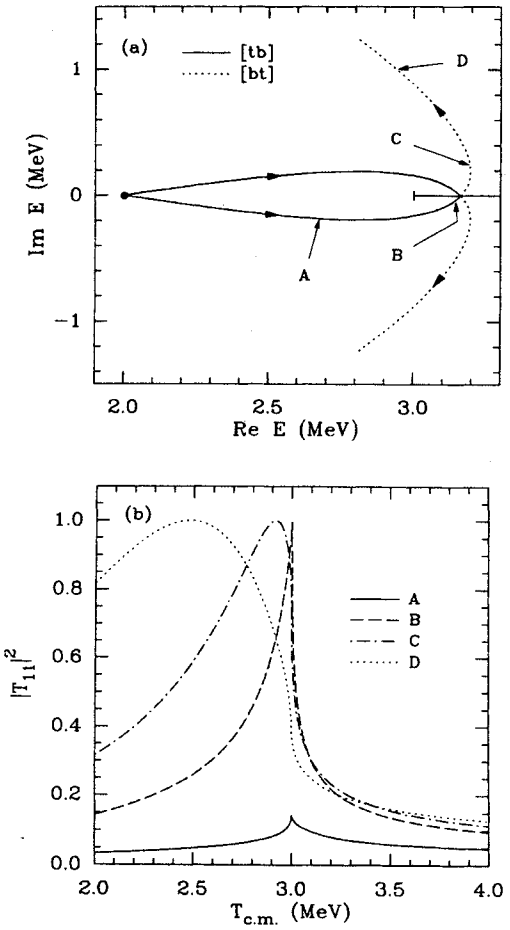

FIG. 2. The pole trajectory (a) and elastic cross section (b) for coupled channels S_1 and S_2. In (a) the position for zero coupling is indicated by the dot and the motion with increasing coupling is in the direction of the arrows. The points labeled A, B, C, and D correspond to similarly labeled curves in (b). The heavy horizontal line indicates the channel-2 threshold cut, $\Theta_2=3$ MeV.

to be only one pole or one to be the conjugate of the other. As the coupling strength is increased from zero this pole moves (with its complex conjugate) into the complex plane on sheet $[tb]$. The motion of this pole with increasing coupling is shown in Fig. 2(a). The dot indicates the position for zero coupling and the arrows show the direction of motion for increasing coupling. We will use this convention for all pole trajectory plots. As can be seen, it eventually crosses the real axis just above the second threshold (the threshold and associated cut are denoted by the heavy horizontal line), crossing from $[tb]$ to $[bt]$. The elastic cross section is plotted in Fig. 2(b) for each of the points A, B, C, and D (corresponding to $\lambda_{12}=0.035$, 0.054, 0.062, and 0.072, respectively) marked on Fig. 2(a). As previously noted,[5] the significance of the pole crossing the two thresholds is that the cusp in the cross section reaches its unitary limit and becomes a rounded peak.

It is interesting to compare this case with one where the antibound state in the second channel is replaced with a bound state. This can be achieved by replacing the second channel parameters of the previous example with the parameter set S_3 from Table II. The pole motion as λ_{12} is increased is shown in Fig. 3. This time the pole–shadow-pole pair begin (for $\lambda_{12}=0$, indicated in the figure by a dot) on sheets $[tt]$ and $[bt]$. As the coupling increases, they move as a conjugate pair onto the $[bt]$ sheet. Eventually they coincide on the real axis below the first threshold and move along the axis in opposite directions. When the one that moves up the real axis reaches the first threshold at zero, it crosses to the $[tt]$ sheet and moves down the real axis as a bound state. This case presents no surprises in the cross section. Since sheet $[bt]$ is close to the physical region, the pole initially shows up as a typical resonance peak in the cross section, showing the usual bound-state behavior once the pole has moved onto the negative real axis.

The first example above illustrated a case where there was a very distinct transition from a cusp in the cross section to a rounded peak which corresponded to the pole moving from the $[tb]$ sheet where it could not be "seen" from the scattering region to sheet $[bt]$ where it could be seen. This seems to be a general principle. A pole near the second threhsold causes a cusp if it is on a sheet far removed from the physical region and a rounded resonance peak if it is near the physical region. The transition from a pole that causes a cusp to one that causes a resonance peak is not always as clear as the case above where the pole changed sheets. The coupled-channel representation of the ΛN-ΣN (or hyperon-nucleon YN) system of Ref. 6 is an example of a case where the transition point is less well determined. The parameter set A of Ref. 6 can be constructed from the sets ΛN_A and ΣN_A in Table II with a coupling strength of 0.079 906 4 and thresholds of 2054.5 MeV for the ΛN channel and 2128.3 MeV for the ΣN. Sets B and C are constructed similarly from ΛN_B and ΣN_B with a coupling of 0.294 999 and from ΛN_C and ΣN_C with a coupling of 1.065 84. The difference between the λ values used here and those from Ref. 6 is due to a difference in the normalization of the propagator and to the slightly different definition of the

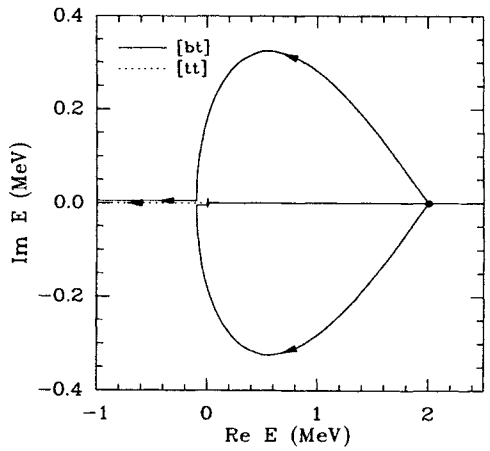

FIG. 3. The pole trajectory for coupled channels S_1 and S_3 with $\Theta_2=3$ MeV. The channel-1 threshold cut at 0 MeV is indicated by the horizontal line.

form factor. We will refer to these three parameter sets as YN_A, YN_B, and YN_C.

In the limit of zero coupling, YN_A is similar to the first example above in that there is initially a channel-2 anti-bound state between the thresholds. However, the close proximity to the threshold and the nearness of the other background poles conspire to produce a somewhat different pole trajectory. As shown in Fig. 4, the pole on $[tb]$ does not cross the axis above the second threshold but instead diverges, presumably to $(\infty, \pm\infty)$. Since the pole on $[tb]$ is far from the physical region but close to the second channel threshold, the channel-1 elastic cross section exhibits a strong cusp behavior at threshold as expected [see Fig. 5(b)].

Of more interest to us is the difference between the parametrizations YN_B and YN_C. These both begin, in the zero-coupling limit, with a bound-state pole from the second channel situated between the two thresholds, differing slightly in the positions of the other poles. The trajectories of the bound-state poles [which move onto sheet $[bt]$ when the coupling is turned on] are shown in Fig. 5(a). The solid curve is YN_B and the dashed curve is YN_C. The points on these trajectories that correspond to the fits of Ref. 6 are shown ($\lambda_{12}=0.295$ for YN_B and $\lambda_{12}=1.066$ for YN_C). The fact that the pole in the YN_B fit is nearer to the physical region than in the YN_C fit, is manifest by the rounded peak in the YN_B cross section and the cusp for YN_C [see Fig. 5(b)]. Actually, the coupling strength used in the parametrization YN_C is almost at the critical value corresponding to the transition from peak to cusp. This is illustrated in Fig. 5(c) where we show the cross section calculated using the coupling strength of 1.065 84 used in Ref. 6 (solid line), and two values on either side of this, namely 0.5 (dashed line) and 1.5 (dotted line). Thus, the nature (cusp or resonance peak) of the structure in the ΛN cross section as one crosses the ΣN threshold, is not determined solely by whether one has, in the zero-coupling limit, a bound state in the ΣN channel.

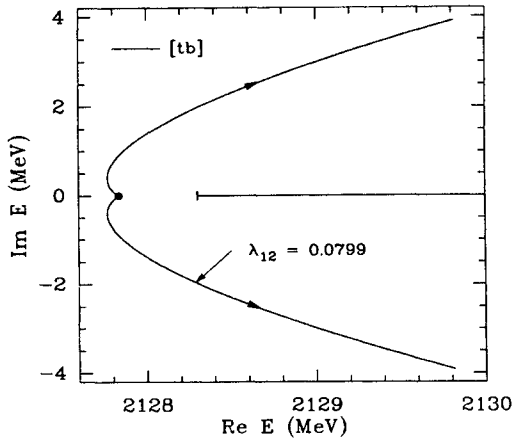

FIG. 4. The pole trajectory for coupled channels ΛN_A and ΣN_A. A coupling of $\lambda_{12}=0.0799$ corresponds to the parametrization of Ref. 6. Also shown is the ΣN threshold cut at 2128.3 MeV.

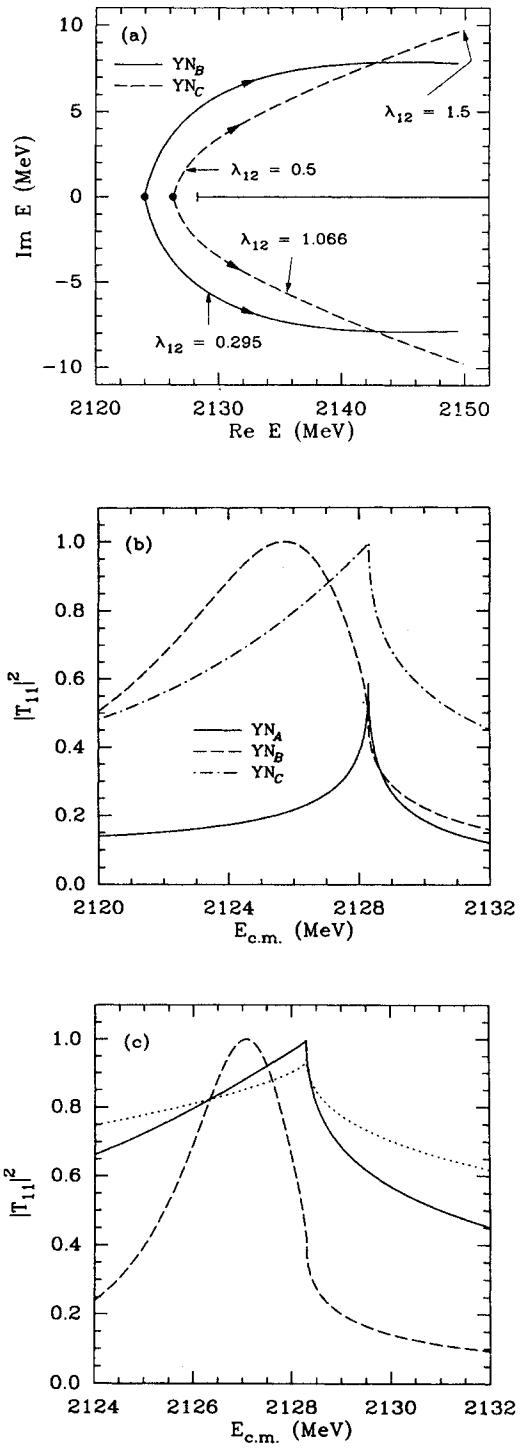

FIG. 5. (a) The pole trajectories for the coupled systems YN_B and YN_C. The ΣN threshold cut at 2128.3 MeV is indicated by the horizontal line. (b) The corresponding elastic cross sections using the fitted coupling strengths from Ref. 6 (0.295 for YN_B and 1.065 84 for YN_C). Also shown is the YN_A cross section which uses a coupling of 0.0799. (c) The YN_C elastic cross section with the coupling set to 1.065 84 (solid line), 0.5 (dashed line), and 1.5 (dotted line). The pole positions for these couplings are indicated in (a).

B. Two coupled p waves

With the form factors we are using, the only way to generate a resonance pole in the complex plane in the single-channel s wave is by using a repulsive potential ($\lambda > 0$). Since a resonance pole arising from a repulsive potential is probably an artifact of the separable potential, the simplest meaningful system in which we can start with poles in the complex plane is two coupled p waves. The configuration we wish to consider is that of a pole slightly above the second channel threshold, originating in either the first or second channel. Parameters which satisfy these criteria are sets P_1, P_2, and P_3 in Table II. The extreme parameter values of sets P_2 and P_3 are necessary in order to achieve such a narrow resonance.

We first consider the consequences of starting with a pole in the first channel just above the threshold of the second channel which has no nearby poles. That is, we use parameter set P_2 for the first channel while for the second channel we use P_1 and a threshold of 1 MeV. The path of the poles for increasing coupling is shown in Fig. 6(a). Initially, for zero coupling, there is a pole on sheet $[bb]$ and its shadow on $[bt]$. (For weak coupling the pole on $[bb]$ is closest to the physical region so we call it the pole and the one on $[bt]$ the shadow pole. For larger coupling, the situation is eventually reversed and we should call the one on $[bb]$ the shadow pole.) As the coupling increases, the pole and its shadow move apart. The most interesting feature of this example is that the shadow pole eventually crosses from sheet $[bt]$ to $[tb]$ at some point above the second threshold. As indicated in Fig. 6(a), for very large coupling, all of the poles eventually approach the first channel threshold at 0 MeV and move down the negative real axis. At the first channel threshold the pole conjugate pair on sheet $[bb]$ move onto sheets $[bb]$ and $[tb]$ while the shadow-pole conjugate pair on $[bt]$ move onto $[tt]$ and $[bt]$.

The fact that the shadow pole can change sheets as the coupling is increased (a feature which appears again in later examples), has an important ramification. That is, it is not possible to determine with which channel the pole is associated by simply knowing on which sheet the shadow pole is situated. Eden and Taylor[1] point out that, in the limit of weak coupling, a pole can be characterized as being produced by a given channel by observing on which sheets the pole and shadow pole appear. Specifically, for weak coupling the poles cannot have moved far from their zero-coupling positions, where the discussion following Eq. (2.15) enables one to determine in which channel the poles originated. However, this example shows that the same conclusions cannot be drawn for strong coupling.

It is interesting to see whether there is some correlation between observables and the position of the shadow pole. Such a correlation can be seen in the phase shifts. In Fig. 6(b) we plot the channel-1 phase shifts for the points marked A, B, and C on Fig. 6(a) ($\lambda_{12}=0.45\times10^{-4}$, 0.55×10^{-4}, and 0.65×10^{-4}) while Fig. 6(c) shows the channel-2 phase shifts. Points A and C correspond to the shadow pole being on sheet $[bt]$ while at point B it is on the $[tb]$ sheet. In this example, the channel-1 phase shifts pass through 90° when the shadow pole is on $[bt]$, but they pass through 0° when it is on $[tb]$. The opposite is true of the channel-2 phases. As required by unitarity,[8] the diagonal S-matrix elements have

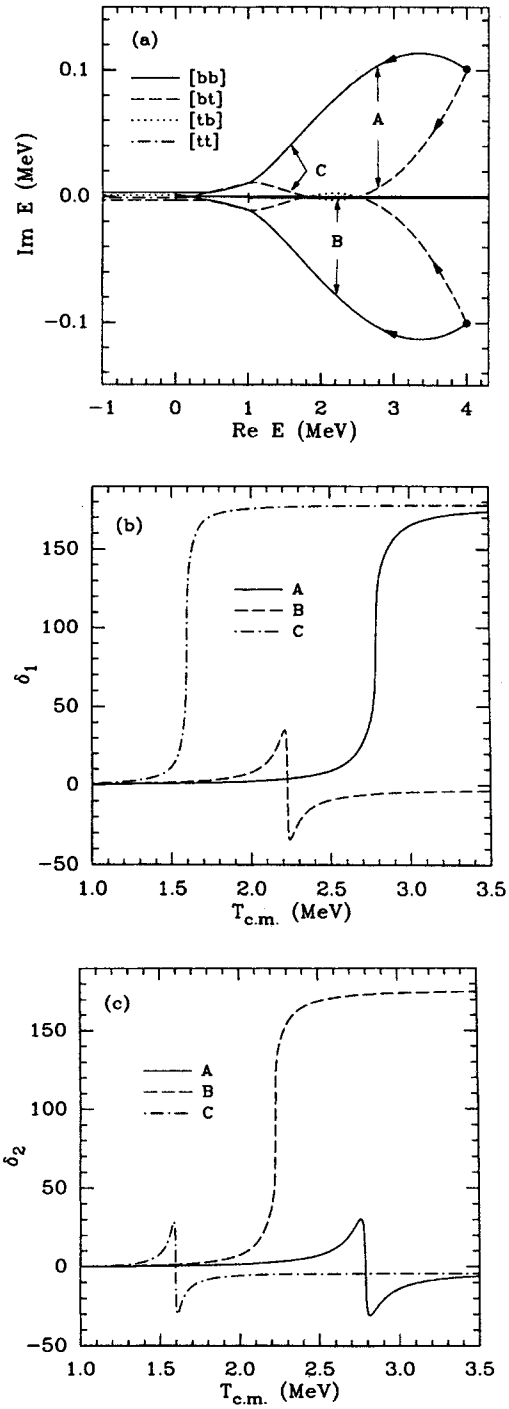

FIG. 6. (a) The pole trajectory for coupled channels P_2 and P_1. The labeled points indicate the pole positions corresponding to similarly labeled curves in (b) and (c). Also shown is the channel-1 threshold cut at 0 MeV and the channel 2 cut at 1 MeV. (b) Channel-1 phase shifts. (c) Channel-2 phase shifts.

a zero at the shadow-pole energy. This is reflected by a zero in the inelasticity when the shadow pole is on the real axis. Also, at this point, the reaction cross section $|T_{12}|^2$ attains its maximum allowed value of $\frac{1}{4}$.

We now consider what happens if the pole is initially generated by the second channel. For this we use parameter set P_1 in channel 1 and set P_3 in channel 2 with the threshold at 1 MeV. In this configuration we have a very similar starting point to the previous example except that the pole at (4.0,±0.1) MeV is now generated by the second channel. This means that the shadow pole begins on [*tb*]. The plot of the pole trajectory is shown in Fig. 7(a). In the limit of large λ_{12}, both the pole and shadow pole approach the first channel threshold. When they reach the threshold, one pole from each conjugate pair remains on that sheet and moves onto the negative real axis, while the other crosses the threshold, hence changing the first sheet label, before moving onto the negative real axis. Eventually there is one pole on the negative real axis for each of the four sheets. Since the pole on [*bb*] will end up on sheets [*bb*] and [*tb*], the shadow pole must be on sheet [*bt*] as it approaches the first threshold to achieve the result of a pole on each sheet along the negative axis. Since it began on sheet [*tb*] it must cross the axis above the second threshold an odd number of times (in this case once). In contrast, in the previous example the shadow pole was already on [*bt*] so it needed to cross above the second threshold an even number of times, or not at all. Hence it is more likely that the shadow pole will cross above the second threshold if the pole is generated by the second channel, than if it is generated by the first.

In Figs. 7(b) and (c) we show the phase shifts in the first and second channels, respectively, at each of the labeled points on Fig. 7(a) (*A*, *B*, *C*, and *D* correspond to $\lambda_{12}=0.6\times10^{-4}$, 0.98×10^{-4}, 1.0×10^{-4}, and 1.4×10^{-4}, respectively). These curves are consistent with our previous hypothesis; namely that the phase shifts of channel 1 pass through 90° when the shadow pole is on [*bt*] while when it is on [*tb*] the phase shifts pass through 0°. Again, the opposite is true of the channel-2 phases.

As our final example of two coupled *p* waves, we consider the case in which there exist poles in both channels in the zero-coupling limit. For this we use parameter set P_4 for the first channel and P_5 for the second with a threshold of 5 MeV. This means the uncoupled system has a broad resonance pole at (5.0,±1.5) MeV generated by the first channel and a narrow pole at (6.0,±0.3) MeV from the second channel. The movement of the poles is illustrated in Fig. 8(a), where the points labeled *A*, *B*, *C*, and *D* correspond to coupling strengths of 0, 0.0005, 0.001, and 0.0025, respectively. With no coupling, the channel-1 amplitude does not see the second channel pole and the phase shifts and Argand diagram exhibit the expected resonance behavior [solid curves of Figs. 8(b) and (c)]. As the coupling is slowly turned on, the effect of the second channel pole and threshold begin to be felt in the first channel amplitude. This effect shows up as a second small loop in the Argand diagram as can be seen in the dashed and dash-dotted curves of Fig. 8. As the coupling increases, the size of the loop grows until it encompasses

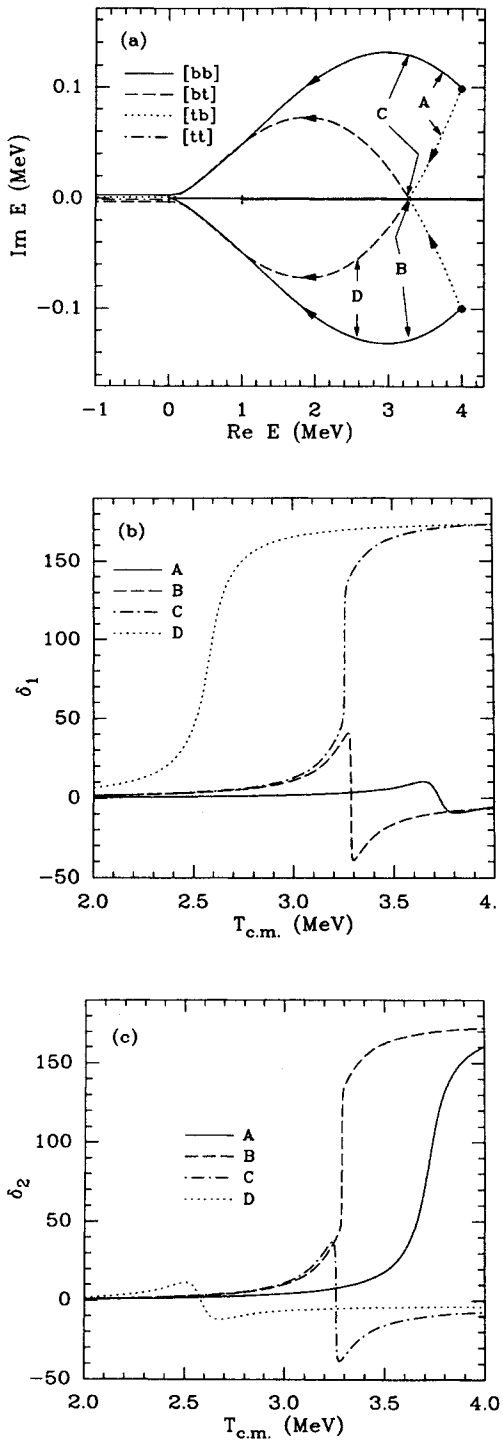

FIG. 7. The same as Fig. 6 but for coupled channels P_1 and P_3.

the point *i*/2. At this stage, which corresponds to the shadow pole of the second channel pole crossing from sheet [*tb*] to [*bt*], the phase shifts shoot rapidly through 180° and 270°.

The structure of the Argand diagram and phase shifts

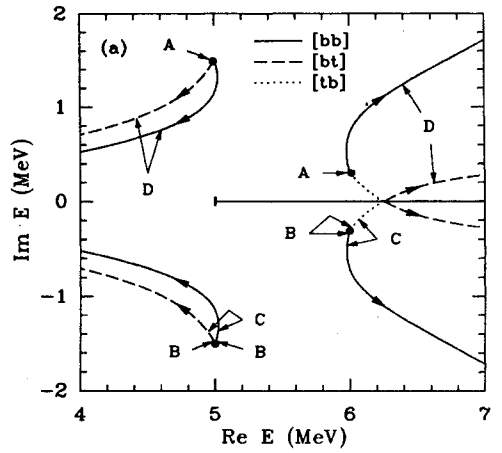

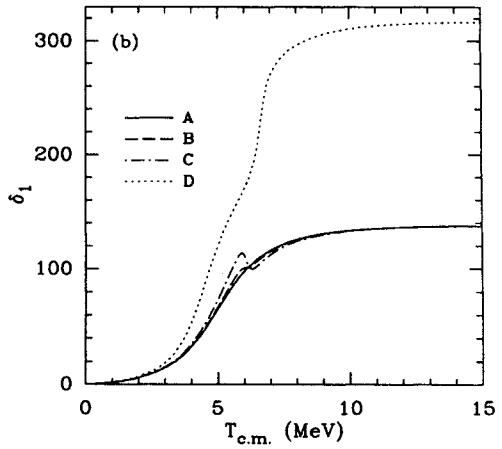

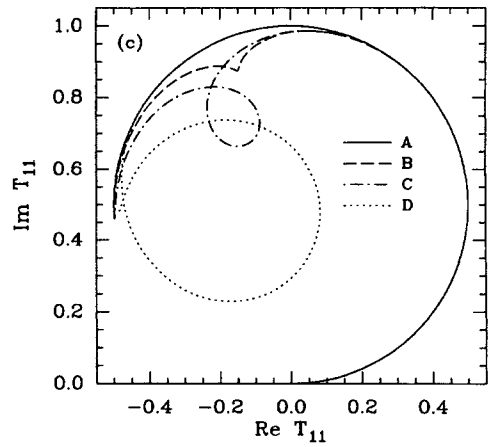

FIG. 8. (a) The pole trajectory for coupled channels P_4 and P_5 with $\Theta_2=5$ MeV. For zero coupling (indicated by dots) there is a pole at (5.0,±1.5) MeV generated by channel 1 and one at (6.0,±0.3) MeV generated by channel 2. The labeled points indicate the positions of these poles for four values of the coupling strength (A corresponds to zero coupling). (b) Channel-1 phase shifts at the coupling strengths indicated in (a). (c) Channel-1 Argand diagram.

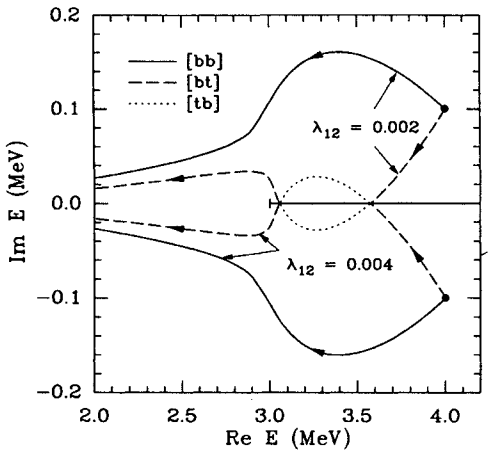

FIG. 9. The pole trajectory for coupled channels D_1 and S_1 with $\Theta_2=3$ MeV.

for small coupling look remarkably similar to the πN P_{11} amplitude[7] in the laboratory energy range of 0–800 MeV. This may suggest that the second looping seen in that case is caused, in part, by a pole originating in the $\pi\Delta$ channel. Of course, the unstable nature of the Δ and the presence of the $\pi\pi N$ and ρN thresholds prevent a direct interpretation in terms of the simple case we have considered here.

C. Coupled *s* and *d* waves

Our interest in the case of coupled s and d waves is primarily to check that the features we have observed with two s waves and two p waves are not just artifacts of those particular choices of angular momentum. To this end, we constructed a model to mimic the first coupled p-wave example above. Channel 1 is a d wave channel (D_1) with a narrow resonance pole a little above the channel-2 threshold which is at 3 MeV. Channel 2 is s wave (S_1) and has no nearby poles. This is, in fact, the structure of the $n\alpha$-dt system considered in Ref. 2. When the coupling is turned on, we see a pattern similar to that observed in the corresponding coupled p-wave example. The paths taken by the pole and shadow pole are illustrated in Fig. 9. We find the same correspondence between the sheet on which the shadow pole lies and whether the phase shifts go through 0° or 90°. Hence we conclude that the observations made while considering p waves where not specific to the angular momentum structure.

IV. CONCLUSIONS

We have adopted a "what happens if . . ." approach to exploring the effect poles on the various Riemann sheets have on the scattering observables. Rather than fitting parameters to a data set and then seeking the poles, we have looked at the inverse question. That is, given a configuration of poles, what are the properties of the resulting amplitudes? This knowledge is helpful in gaining

an intuitive picture of the physics that may underly a particular set of observables.

Let us summarize what has been learned from this investigation. First, we observe that, as the coupling strength is varied, the shadow pole is free to cross the real axis above the second channel threshold. For example, if we start with a pole on $[bb]$ above the second channel threshold and its shadow on $[bt]$ ($[tb]$) then, for some value of the coupling, the shadow pole can cross from $[bt]$ to $[tb]$ ($[tb]$ to $[bt]$). This implies that the channel in which the pole exists in the zero-coupling limit cannot be inferred from the sheets on which the poles appear in the strong-coupling regime. This does not contradict the result of Eden and Taylor[1] but merely emphasizes that it is only in the weak-coupling limit that such an inference can be drawn. As a consequence, it is not possible to determine from the R-matrix parametrization of Ref. 2, whether it is the $n\alpha$ or dt channel that is responsible for the $J^{\pi}=\frac{3}{2}^{+}$ resonance in ^{5}He.

We observe that, as the shadow pole changes sheets, the phase shift undergoes a transition from passing through 0° to passing through 90°. This transition is a reflection of whether the loop in the Argand diagram passes above or below the point $i/2$. The point $i/2$ corresponds to a zero in the diagonal S-matrix elements. As noted by Kato,[8] unitarity constraints imply that a pole on an unphysical sheet is accompanied by a zero in the diagonal S-matrix elements on the physical sheet. Hence, when the shadow pole is on the real axis, the Argand diagram trajectory passes through the point $i/2$. This means that the signature of a narrow pole on a sheet far removed from the physical region is large inelasticity (i.e., $\eta \approx 0$).

We only find strong cusp effects in the cross section at the opening of a new channel when there is a nearby pole associated with that channel on an unphysical sheet that is far from the physical region. If the pole lies sufficiently close to the physical region, then a rounded resonance peak appears instead of a cusp. If the pole resides on sheet $[bt]$ and below the second threshold, then it is close to the physical region and it will produce a rounded resonance peak. If it is far above the second threshold on that sheet, then it lies far from the physical region and will produce a cusp. Between these extremes is a gray area where it is not obvious whether the effect will be cusp or peak. However, in the $K^{-}d \rightarrow \pi N \Lambda$ reaction, the existence of a ΣN bound state in the absence of ΛN-ΣN coupling cannot be inferred from the cusp-peak nature of the cross section at the ΣN threshold.

Finally, we observe that a small loop in the Argand diagram superimposed on a larger, typical resonance loop (such as that observed in the Karlsruhe-Helsinki P_{11} πN amplitude[7]) can be generated from two weakly coupled channels that each have resonance poles in the uncoupled limit. Increasing the coupling in such a system can lead to phase shifts that pass rapidly through 90°, 180°, and 270°.

ACKNOWLEDGMENTS

We wish to express our gratitude to G. M. Hale for bringing the shadow pole question to our attention and for several enlightening discussions during the course of this work. This research was performed under the auspices of the U.S. Department of Energy.

*Present address: TRIUMF, 4004 Wesbrook Mall, Vancouver, B.C., Canada V6T 2A3.

[1]R. J. Eden and J. R. Taylor, Phys. Rev. **133**, B1575 (1964).
[2]G. M. Hale, R. E. Brown, and N. Jarmie, Phys. Rev. Lett. **59**, 763 (1987).
[3]I. Lovas and E. Dénes, Phys. Rev. C **7**, 937 (1973).
[4]W. M. Kloet and J. A. Tjon, Nucl. Phys. **A392**, 271 (1983).
[5]W. R. Frazer and A. W. Hendry, Phys. Rev. **134**, B1307 (1964).
[6]G. Toker, A. Gal, and J. M. Eisenberg, Nucl. Phys. **A362**, 405 (1981).
[7]G. Höhler, F. Kaiser, R. Koch, and E. Pietarinen, *Handbook of Pion-Nucleon Scattering* (Fachinformationszentrum Karlsruhe, Germany, 1979).
[8]M. Kato, Ann. Phys. (N.Y.) **31**, 130 (1965).